Biosensors and Bioelectronics 219 (2023) 114822

Contents lists available at ScienceDirect

Biosensors and Bioelectronics

journal homepage: www.elsevier.com/locate/bios

Combining plasmon-enhanced fluorescence with Rayleigh surface acoustic waves to quantify Carcinoembryonic Antigen from human plasma

Yuqi Huang, Shuangming Li, Venkat Bhethanabotla *

Department of Chemical, Biological, and Materials Engineering, University of South Florida, Tampa, FL, 33620, USA

ARTICLE INFO

Keywords:
Surface acoustic wave
Metal-enhanced fluorescence
CEA
Non-specific binding
Immunofluorescence

ABSTRACT

To improve the direct quantification of Carcinoembryonic Antigen (CEA) from body fluids by immunofluorescence, a surface acoustic wave (SAW) based biosensor was developed combined with an optimized silver nanostructure at the sensing region. Fluorescence signal amplification is achieved by patterning silver nanostructures using the rapid thermal annealing (RTA) method. In addition, the problem of background noise interference from nonspecific binding in human plasma is addressed by Rayleigh wave streaming at the immunoassay region, which shows a reduction in the limit of detection. The results show that the silver nanostructures significantly increase the sensor sensitivity by 49.99-fold and lower the limit of detection of CEA in phosphate buffered saline (PBS) solution to 101.94 pg/mL. The limit of detection of CEA biomarker in human plasma was successfully brought down to 11.81 ng/mL by reducing background noise using Rayleigh SAW streaming. This allows for a point-of-need sensor system to be realized in various clinical biosensing applications.

1. Introduction

Carcinoembryonic antigen (CEA) is a cancer-related prognostic biomarker. The CEA level can increase in various cancer types, such as colon, pancreatic, and ovarian cancers (Duffy, 2001; Lertkhachonsuk et al., 2020; Meng et al., 2017). It is important for early diagnosis of cancer biomarkers to provide timely treatment during the early stages of cancer. Traditional detection methods for CEA including test strips (Diagnostics, 2022), enzyme-linked immunosorbent assay (ELISA), and mass spectrometry (Choi et al., 2014), are not capable of point-of-care detection in clinically significant CEA level that allows long-term tracking for patient's health condition. These techniques have disadvantages such as a high limit of detection, long operation time, high instrument cost, and trained personnel required. For these reasons, a rapid and sensitive point-of-care biosensor is needed to address the issue for the clinical purpose of cancer biomarker detection.

Immunofluorescence (IF) assay is an immunoassay method for real time biomarker sensing. It often requires fluorophore-labeled antibodies to examine antibody-specific antigens (Odell and Cook, 2013). IF has been a popular technique in immunohistochemistry because the visualization of antibody-antigen interaction can be examined quantitatively. However, one of the long-existing problems for IF assay is the nonspecific binding from unwanted substances, which induces background signal to the assay and obstructs low limits of detection (LOD). Most known techniques to improve the quality of IF assay have been focusing on amplifying the signal and reducing nonspecific binding (Bohlool and Schmidt, 1968; Buchwalow et al., 2011; Chao et al., 1996; Cho et al., 2020; Ness et al., 2003). Metallic nanoparticles, such as silver and gold, can interact with fluorophores at an excited state and cause surface plasmon resonance (Lakowicz, 2006). This interaction results in several effects on fluorescence, such as changes in the emission spectrum, enhanced photostability and increased quantum yields, which are generally depicted as metal-enhanced fluorescence (MEF) (Lakowicz, 2006).

Various studies have been done to utilize MEF sensing for biological samples, such as DNA, proteins, and aptamers, as reviewed by Jeong et al., (2018). For surface-based immunofluorescence assays, there are several surface modification methods to achieve the MEF effect. Our group has studied solvent-based CF_3COOAg-precursor synthesized silver nanocubes, which demonstrates CEA quantification level of 1 ng/mL (Liu et al., 2018). However, solvent-based techniques such as growing colloidal suspension have drawbacks of difficulties for scaled up production of monodispersed metal particles with uniform spacings, and often the MEF effect can be affected by detached metal nanoparticles during the assay (Jeong et al., 2018; Liu et al., 2018). Other advanced patterning techniques for MEF include electron-beam lithography and

* Corresponding author.
E-mail address: bhethana@usf.edu (V. Bhethanabotla).

https://doi.org/10.1016/j.bios.2022.114822
Received 5 April 2022; Received in revised form 1 August 2022; Accepted 14 October 2022
Available online 18 October 2022

laser/ion beam machining. These techniques provide great control over the geometry, size, height, and spacing between metal nanoparticles. However, they are very expensive and not widely accessible, and their beam writing speeds make them difficult to achieve large-scale nanostructure fabrication required for biosensing (Li and Bhethanabotla, 2021). To address these issues, rapid thermal annealing (RTA) process has been described in a previous publication in our group (Li and Bhethanabotla, 2021). The optimized silver nanoparticle (AgNP) coated with a silica film can produce significant fluorescence enhancement to the antibody-antigen immunoassay (Li and Bhethanabotla, 2021).

Another long-existing problem that can affect biosensor performance is the non-specific binding (NSB) protein deposition onto the sensor surface. NSB proteins can adhere to the immobilized antibodies, thus reducing the sensitivity and specificity of immunoassay (Lichtenberg et al., 2019). The most popular practice to prevent NSB protein adhesion in enzyme-based immunoassay is to apply bovine serum albumins (BSA) or non-fat dry milk (Lichtenberg et al., 2019). However, there are reports that show NSB proteins can still adhere to these blockers, and their efficiencies on NSB blocking is often dependent on the type of selected antigen-antibody pair, surface materials, and surface hydrophobicities (Ahirwar et al., 2015; Jeyachandran et al., 2010; Lichtenberg et al., 2019). Especially when dealing with human bio-matrices such as blood, serum, and plasma, the concentrations of non-specific proteins and molecules from these samples are orders of magnitude higher than the target biomarkers presented (Vaidyanathan et al., 2015). Therefore, a huge challenge of direct quantification in body fluids with the enzyme-linked immunoassay method is the false signal resulting by such high concentrations of non-specific proteins and molecules (Vaidyanathan et al., 2015). To address this issue, our previous studies have demonstrated that the Rayleigh surface acoustic wave (SAW) can effectively remove non-specifically bound (NSB) proteins in immunoassays (Cular et al., 2008; Huang et al., 2021; Liu et al., 2018). When Rayleigh wave is propagating along a certain direction in the piezoelectric device and comes in contact with the sample liquid, wave energy is transferred to the liquid domain and causes acoustic streaming (Das et al., 2020; Sankaranarayanan et al., 2008). Sankaranarayanan et al. presented a coupled-field fluid-structure interaction (FSI) model that simulates distortions of the lithium niobate substrate, which shows that the drag and lift forces from SAW streaming can lead to separation of NSB proteins from solid substrate. The roles of higher applied power and higher frequency in having increased streaming velocity to achieve higher removal efficiency are also stressed (Sankaranarayanan et al., 2008).

In this work, we combine the effect of MEF for fluorescence signal enhancement and Rayleigh SAW streaming for NSB removal in a single sensor device to quantify CEA directly from human plasma. The silver nanoparticles generated from RTA by annealing a thin silver film presented as a better substitute compared to the CF_3COOAg-precursor or colloidal synthesis procedure, yielding a relatively uniform nanoparticle distribution and better adhesiveness to the substrate. The thermally annealed silver film was then coated with a thin silica layer to protect the AgNPs as well as optimize the plasmonic enhancement by minimizing the quenching effect (Li and Bhethanabotla, 2021). Details of the design and fabrication of the SAW device can be found in the supplemental section S6. A sandwich immunoassay involving capture and detection CEA antibodies was conducted within the plasmonic region on the SAW substrate, and the limit of detection of CEA in human plasma was successfully decreased to 11.81 ng/mL due to fluorescence signal enhancement and NSB proteins removal. These developments provide solutions to the persistent issue of biofouling, getting us closer to a small-scale, easy-to-operate, point-of-need detection system for cancer biomarkers at clinically relevant level from a small volume of blood sample.

2. Simulation and experimental validation of metal-enhanced fluorescence

The fluorescence intensity from a specific fluorophore is determined by the emission rate γ_{emi}, which is expressed as (Ansys/Lumerical, 2021; Bharadwaj and Novotny, 2007):

$$\gamma emi = \gamma exc \cdot Q$$

Where the emission rate is the product of, γ_{exc}, which is the excitation rate and is related to the local electric field and transition dipole moment, and Q is the quantum yield, which is the efficiency of photon emission. The expressions for solely quantum yield (Q_0), and the quantum yield when a metal nanoparticle comes close to the fluorophore (Q_m) can be expressed as: (Lakowicz, 2006)

$$Q_0 = \Gamma \ / \ (\Gamma + k_{nr})$$

$$Q_m = (\Gamma + \Gamma_m) \ / \ (\Gamma + \Gamma_m + k_{nr})$$

Where Γ and Γ_m are respectively, the radiative decay rates with and without metal nanoparticle structure, and k_{nr} is the non-radiative rate in the system. The interaction of a proximate metal structure to the fluorophore increases the quantum yield Q by adding the metal-induced radiative decay rate Γ_m.

Although numerous experimental studies have been done on the effect of fluorescence enhancement from the addition of nanoscale metallic nanostructures, few have reported the relationship between the nanostructure geometry and fluorescent enhancement, due to the complexity and resources needed to conduct these experiments. In this study, Finite Different Time-Domain (FDTD) simulations were performed to predict the fluorescence enhancement of a fluorophore interacting with silver nanoparticle structures. FDTD is a useful tool to simulate the radiative and non-radiative decay rates for a metallic structure with a radius smaller than the excitation wavelength (Ansys/Lumerical, 2021). In this study, the AgNPs from the annealed silver film have an average radius of 20–160 nm (supplemental material S1), which is much smaller than the simulated spectra from 400 to 650 nm. Fig. 1-a, shows a schematic illustration of the FDTD simulation model. The silver nanostructures used in FDTD were created by importing SEM images of annealed silver films from a range of 5–20 nm thickness, and the fluorophore placed above metal nanostructures is represented by a dipole radiation emitter. The distance between silver nanoparticles and dipole (D = 35 nm) was selected for simulation, which was based on the 10 nm silica layer with different types of IgGs layouts in between fluorophore and silver nanoparticles (Liu et al., 2018). The estimated thicknesses of silver nanoparticles T used for simulations were calculated by the ratios of deposited silver film thicknesses over covered area fraction (Supplement data, S1). After simulation is complete, the enhancement factors were calculated based on the ratio between the total decay rates of substrates with and without plasmonic structures. Fig. 1b shows that the enhancement factor is dependent on the particle geometry, as the silver film thickness increases from 0 nm to 15 nm, the enhancement factor for the analyzed spectra starts to increase. The optimized silver nanoparticles of the annealed 15 nm silver film produce the highest fluorescence enhancement of 2.29, which occurs at the wavelength of 452 nm. It is noticed that silver nanoparticles for annealed film thicknesses at 20 nm and 25 nm result in a fluorescence decrease, which is possibly due to over-deposited silver films failing to produce nanoparticles and the remaining flat silver film acting as a mirror to hinder the plasmonic effect. Silver nanoparticles from annealed film thicknesses of 5–25 nm were also tested with fluorescence immunoassay to compare with FDTD simulation, with fluorescent images in supplemental data S3. Nanoparticles fabrication and immunoassay protocols are same from the experimental procedures in section 3.2 and 3.3, and the tested CEA antigen concentration is at 1 ng/mL in PBS buffer. The fluorescence intensities were acquired using calculated

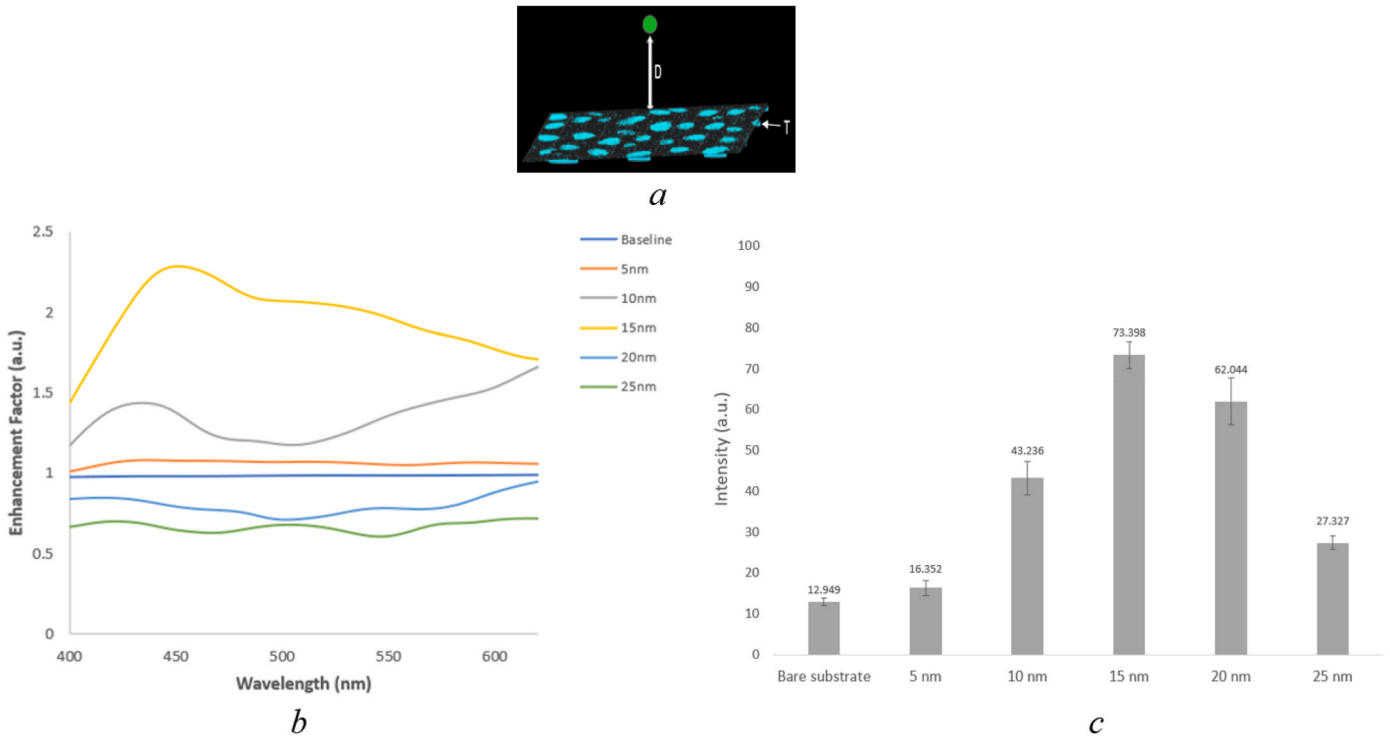

Fig. 1. a) Schematic of FDTD simulation; b) FDTD simulated enhancement factor for annealed silver film thicknesses of 5–25 nm; c) Fluorescence intensities from AgNPs at deposited thicknesses of 0 nm, 5 nm, 10 nm, 15 nm, 20 nm, and 25 nm.

green channel values of the RGB system (255,255,255) through the all-field of view of fluorescent images. Results in Fig. 1-c shows that the surface without coated AgNPs has a fluorescent intensity of 12.949 (255 units maximum), and AgNPs nanostructures from all 5–25 nm films can enhance fluorescent intensities. The 15 nm nanostructures optimized the enhanced fluorescence signal by a factor of 5.67. Although experimental data of 20 nm and 25 nm nanostructures also show fluorescence enhancements, both FDTD simulation and experimental indicate that the fluorescence enhancement is optimal for the 15 nm silver film samples. Therefore the 15 nm film is selected for the fabrication of SAW devices.

3. Experimental

3.1. Reagents and apparatus

The following materials were used in these experiments: (3-Aminopropyl) triethoxysilane (APTES, Sigma-Aldrich), CEA capture antibody (Fitzgerald, 10-C10D), CEA detection antibody labeled with Alexa-488 (Fitzgerald, 10-C10E) (tagged with Alexa Fluor 488 Protein Labeling Kit, Thermo Fisher), CEA antigen (Abcam, ab742), PBS (Life Technologies, pH 7.4), bovine serum albumin (BSA, Fisher Scientific), Protein A (abcam), Single Donor Human Plasma (whole blood-derived, Innovative Research, Inc), and deionized water with 18.2 MΩ cm resistivity produced using a Millipore system.

The following instruments were utilized in these experiments: Thermo Scientific Evolution 201 UV–Vis Spectrophotometer, Hitachi S800 Scanning Electron Microscope, Nikon Eclipse FN1 fluorescence microscope, Copper Mountain S5045 Vector Network Analyzer, and Rohde & Schwarz SMA100A signal generator. Silver nanoparticles and antibody functionalized surfaces were analyzed using Veeco Dimension 3000 Atomic Force Microscope (AFM) and Hitachi SU 70 Field-emission SEM.

3.2. SAW device with the plasmonic sensing region

The Rayleigh SAW wave device was fabricated on a 4-inch 0.5 mm 128° YX lithium niobate wafer. The two interdigital transducers (IDTs) consisting of 60 finger pairs with an electrode width of 10 μm and wavelength of 40 μm were fabricated using standard lithography with a negative photoresist. The fabricated SAW devices can generate Rayleigh waves with a fundamental frequency at 98 MHz. Between the two IDTs is the delay-line sensing region of 8 mm × 2 mm, where the plasmonic sensing region with a radius of 2 mm is fabricated at the center of the delay line. The metal nanoparticle sensing region was fabricated using the following steps. First, a silver layer of 15 nm was deposited using E-beam evaporator (AJA 1800 Thin Film Deposition System, AJA International Inc.) at a rate of 0.2 Å/s on piranha cleaned SAW devices. The chips were then treated by an RTA process in which they were rapidly heated to 500 °C in 5 s and remained at this temperature for 1 min. Then, the chips were cooled down to room temperature. The thermal annealing process was performed in an MTI rapid thermal processor. Then a 10 nm silica film was coated on top of the AgNPs to protect them and provide spacing between AgNPs and fluorophores. The same processes were applied on the glass substrate to generate SEM images for annealed 5–20 nm silver films, and the images were imported to FDTD to simulate AgNP structures. By comparison, (SEM images in S2) AgNPs annealed on a lithium niobate sample have a more regular shape, better mono-dispersity, and higher particle density compared than those on a glass substrate. Using ImageJ, the average particle diameter for AgNPs on lithium niobate is calculated to be 209.16 nm, which is similar to the average size of AgNPs formed on glass (215.78 nm). The characteristics of SAW devices were measured with a vector network analyzer (Copper Mountain S5045). Before adding the plasmonic region to the delay line, the SAW devices have fundamental frequencies of about 98 MHz. After adding the plasmonic region, there is a small shift of fundamental frequencies of about 0.1 MHz, and the insertion loss parameters measured as S21 parameter increased from an average of -8dB to −13dB, as shown in supplemental material S8. The increased insertion losses are due to

the damping of the Rayleigh wave into the plasmonic structures. Therefore, the input from the RF signal generator was set to 16 dBm to generate at least 2 mW RF power for NSB protein removal experiments.

3.3. Immunofluorescence assays

Sandwich Immunoassay involving CEA capture antibody, CEA detection antibody, and CEA antigen are assembled on fabricated SAW devices that were pre-cleaned by acetone, methanol, and DI water followed by oxygen plasma treatment. 10 mM 3-APTES in pure alcohol was added to cover the entire chip surface for 1 h and then washed with pure ethyl alcohol (3 × 3min). Then, 30 μL of Protein A at 100 μg/mL was incubated to the surface for 2 h to bind the Fc region of CEA capture antibody, after which the chips were rinsed with PBS (3 × 3min), then dried with nitrogen gas. Washing and drying were performed in all future steps unless otherwise specified. The functionalized surface was incubated with 30 μL of CEA capture antibody at a concentration of 30 μg/mL. After that, non-specific sites were blocked by soaking the chip surface in 1% BSA for 1 h at room temperature. Serial dilutions of CEA antigen in PBS and human plasma samples were prepared in the concentration range of 10 pg/mL to 10 μg/mL. After blocking, 20 μL of CEA antigens were added to the chip surface and incubated for 1 h at room temperature. Finally, 10 μL of CEA detection antibody labeled with Alexa fluorophore 488, at a concentration of 10 μg/mL, was added and incubated for 1 h at room temperature. After washing, a Nikon FN1 fluorescence microscope was used for measurements of fluorescence intensities.

Similar bio-assembly steps were done to measure the plasmonic enhancement and SAW removal effect. The effect of plasmonic enhancement was studied by comparing substrates with and without the plasmonic region, and the CEA antigen samples in PBS solution with a concentration range of 10 pg/mL to 10 μg/mL were quantified. The second experiment compares the performance of the plasmonic sensor to quantify CEA samples diluted in human plasma, and the effect of NSB interference from complex protein mixture (human plasma) is studied. The third experiment was designed to introduce Rayleigh SAW streaming to achieve NSB protein removal. The streaming effect was studied on SAW chips that were modified with AgNP plasmonic region. After adding 10 μL PBS to the CEA antigen incubated surface, the SAW chips were connected to the RF signal generator, and SAW streaming was done by ± 1 MHz sweeping at the fundamental frequency at 98 MHz, with a power of 16 dBm. After streaming the plasmonic regions for 10 min, the fluorophore-labeled CEA detection antibody was added to bind with the CEA antigen. All experiments described above were repeated at least three times for each CEA concentration in order to obtain signal fluctuation noises. Fig. 2 shows the schematic diagram of the CEA immunofluorescence assay.

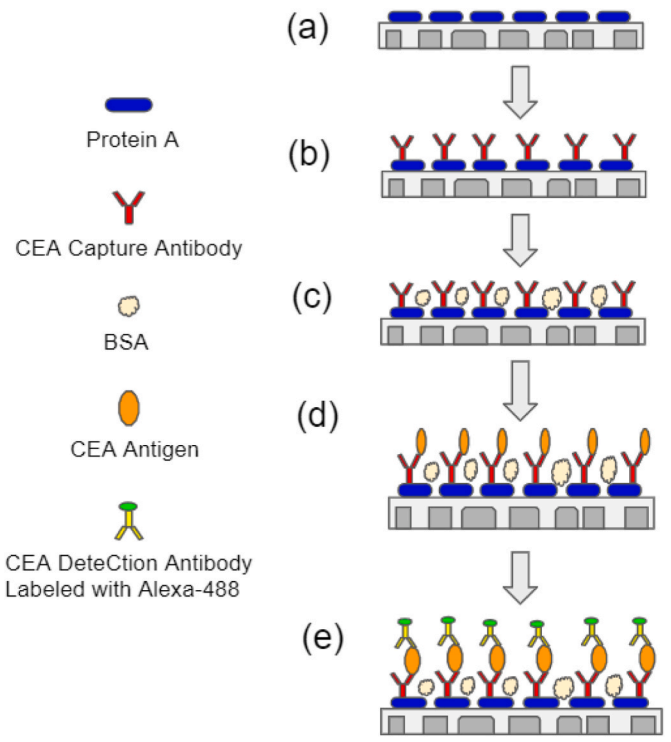

Fig. 2. Procedure for sandwich immunofluorescence assay for CEA quantification; (a) Protein A is assembled on APTES silanized structure; (b) CEA capture antibody is bound to protein A; (c) BSA blocking the unbound sites; (d) CEA antigen bind to capture antibody; (e) Alexa-488 labeled CEA detection antibody bind to CEA antigen.

4. Results and discussion

4.1. Surface morphology of SAW device

The surface morphology features of SAW devices with respected to bare lithium niobate substrate, plasmonic region with AgNPs structures and silica layer, sandwich immunoassay functionalized surface with blood plasma sample, and sandwich immunoassay of SAW treated blood plasma sample are shown in Fig. 3. The RMS roughness of the bare lithium niobate surface was 0.54 nm as in Fig. 3-a. After fabrication of AgNPs with silica layer, the annealed nanoparticles are clearly visible with 3D AFM image (Fig. 3-b), and the RMS roughness increased to 16.58 nm. In Fig. 3-c, it is shown that the roughness increased to 21.11 nm after surface functionalization with antibodies and CEA samples in blood plasma, and the AgNPs were heavily coated with immobilized protein A, BSA blocking agent, antibodies/antigens, and complex proteins non-specifically bound to sensing region. In comparison to Fig. 3-d, with same immunoassay procedures as in Fig. 3-c, the RMS roughness shows a reduction in value due to the SAW streaming, which is 19.90 nm. Other AFM parameters, such as depth at maximum frequency, Z range, mean roughness, and maximum peak/depth, are consistent with RMS roughness reported above. All AFM data and Field Emission-SEM images can be found in supplemental materials S9, S10 and S11. This trend of variation on different samples due to protein immobilization is also consistent with other reported literature data (Galli et al., 2002; Grimaldi et al., 2016; Lamanna et al., 2020).

4.2. Fluorescence enhancement from AgNP plasmonic region

All fluorescence images were obtained by using a Nikon FN1 fluorescence microscope at 10s exposure time. The fluorescence images were processed with ImageJ software to acquire green channel values through all-field of view of the RGB system (255, 255, 255), and the fluorescence intensities with respect to a concentration range of CEA antigen from 10 pg/mL to 10 μg/mL were plotted to form the sensor calibration curve. The fluorescence signal is linear along the logarithm scale of concentration over the range of 0.01–10000 ng/mL, and the sensitivity within the plasmonic region is about 50 times higher than without MEF. Fluorescence results for the control group show that the limit of detection is larger than 1 μg/mL. For samples with plasmonic structures, the signal intensity increases with concentration, with the difference between the 100 pg/mL group and the 1 ng/mL group being clearly distinguishable, as shown in Fig. 4. The limit of detection with plasmonic enhanced fluorescence was established as 101.94 pg/mL, which corresponds to CEA concentration of 3 times the fluctuation noise (Long and Winefordner, 1983). The results show that a silver nanoparticle-modified plasmonic structure can improve immunofluorescence assay results by lowering the limit of detection and enhancing the fluorescence signal. These results are promising and indicate further possibility in achieving single picogram per mL limit of detection with optimized plasmonic structures.

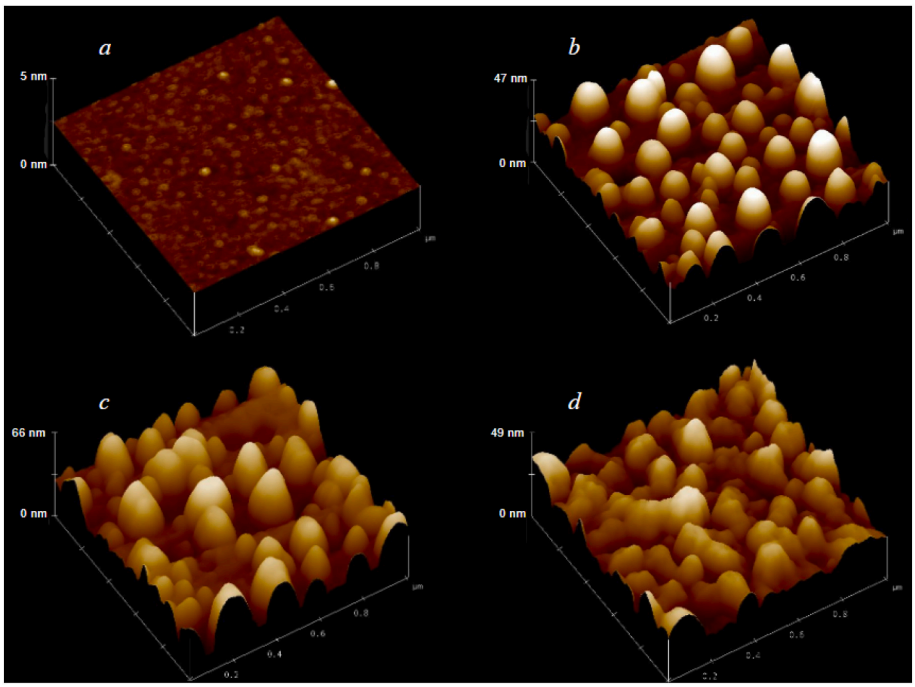

Fig. 3. 3D topographic AFM images a) Bare lithium niobate substrate; b) AgNPs with silica layer; c) Immunoassay-functionalized substrate with CEA in blood plasma without SAW treatment-, and d) SAW treated sample.

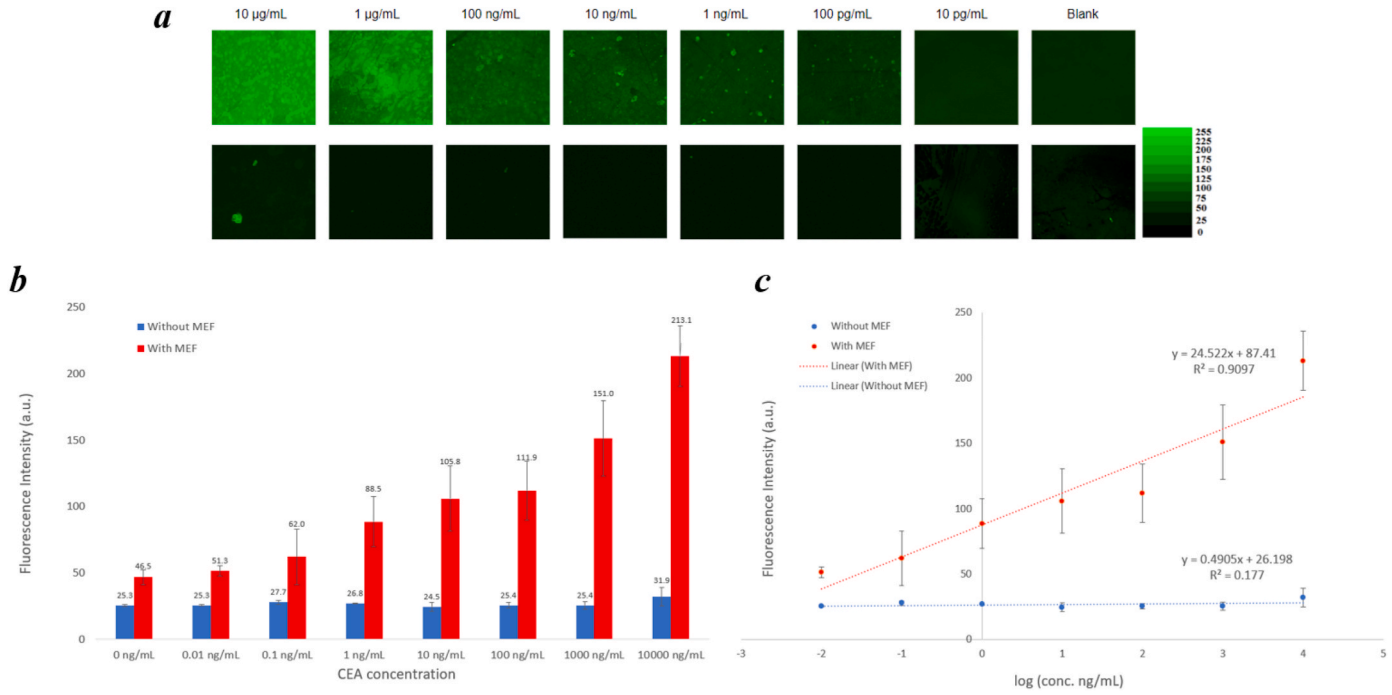

Fig. 4. Results of MEF experiments for CEA diluted in PBS: a) fluorescence images. Top row of images are fluorescence images with AgNPs from 15 nm annealed silver film, and bottom row of images are corresponding controls. CEA concentrations used were 10 µg/mL, 1 µg/mL, 100 ng/mL, 10 ng/mL, 1 ng/mL, 100 pg/mL, 10 pg/mL, and blank PBS sample; b) fluorescence intensities; c) calibration curve for logarithmic concentration of CEA from 0.01 to 10000 ng/mL, the standard deviation is shown in the reported error bars.

4.3. NSB interference from human plasma

To investigate the plasmonic region's performance when non-specific proteins bind to the sensing surface, the CEA antigens were diluted in whole blood-derived human plasma from a single donor (Innovative Research Inc.) to a range of 0.5–5000 ng/mL. Similar immunoassay procedures from the experimental section with CEA in PBS were followed, and the fluorescence intensities on substrates with and without plasmonic structures were measured. Even though MEF substrate can largely enhance the detection capabilities of CEA in PBS with a limit of detection at about 100 pg/mL, quantification of CEA in human plasma is far away from reaching the clinically relevant

concentration of a single nanogram per milliliter level. The signals at and below 50 ng/mL are not measurable even with MEF (Fig. 5a and b). The reasonable explanation for this worsening of the limit of detection is that the complex protein mixture from plasma can cover the CEA specific binding sites of CEA capture antibody by non-specific binding, therefore reducing the available CEA antigens and causing non-specific binding between detection antibodies and background proteins. Eventually, the fluorescence noise level is raised. Fluorescence intensities for all concentrations have been decreased from these data. We can see that without MEF, it is not possible to detect any noticeable signal change of CEA antigen concentrations from all control groups. By improving the fluorescence signal with plasmonic enhancement, the limit of detection of CEA in human plasma is 58.26 ng/mL and we cannot achieve the low limit of detection of CEA diluted in PBS of 0.1 ng/mL. We note that non-specific binding has already been addressed by blocking with BSA, and all washing and rinsing described in the experimental section were followed, except for not using acoustic streaming to remove the NSB proteins.

4.4. Non-specific binding removal using Rayleigh SAW streaming

To assess the removal ability of Rayleigh surface acoustic waves, two sets of experiments were performed. The first group has 10 μL of PBS solution added to the plasmonic region after CEA incubation and was sitting for 10 min without SAW streaming. The second group has 10 μL of PBS added to the MEF region on each chip with streaming at 16 dBm power for 10 min. After which, all chips were washed with PBS 3 times, for 3 min each, and dried with nitrogen gas. The experimental procedures for CEA in plasma test were conducted with identical steps except there was no SAW streaming step added in the previous experiments. Fluorophore labeled detection antibody was then added to the MEF regions for 1 h incubation and then dried, and fluorescence intensity was measured with the microscope, with results shown in Fig. 6a and b. In the previous section we have seen that, although MEF enhances the limit of detection of CEA in PBS to sub-nanogram level, non-specific binding can greatly interfere with the fluorescence signal when detecting from plasma samples. However, with the same experimental conditions, the limit of detection can be reduced when SAW streaming was applied, and the linear trend is observed from 0.5 ng/mL to 5000 ng/mL, as shown in Fig. 6c and d. These results are in good agreement with our theoretical studies reported previously, that is, the weak binding forces of NSB can be overcome with SAW-induced drag and lift forces in fluid, which causes biofouling removal and prevents particle reattachment, and therefore improve sensing response (Sankaranarayanan et al., 2010), as illustrated in Fig. 6e. Especially, effective removal can be achieved in higher SAW streaming frequencies and higher acoustic power (Sankaranarayanan et al., 2010). By using the finite element fluid solid interaction model for simulation, Sankaranarayanan et al. found that the minimum protein radius of 16 nm can be removed with 100 MHz Rayleigh SAW at 1 V peak-to-peak (4 dBm) on a YZ-$LiNbO_3$ substrate, and this removable particles radius can be decreased to 1 nm when this power surpasses 5 V (18 dBm) (Sankaranarayanan et al., 2010). In this experiment, peak-to-peak voltage of around 1 V was applied for a relatively mild SAW streaming. However, there were also an average of 10.91% fluorescence intensity decrease, which indicates that a certain amount of target antigens and specific pairs could be removed due to the SAW streaming, causing the decrease in signal for all concentration group. The SAW removal group has the limit of detection established at 11.81 ng/mL(Long and Winefordner, 1983).

5. Conclusions

In this work, a novel CEA antigen quantification approach via immunofluorescence is demonstrated. By combining functionalities of surface acoustic wave-based removal of non-specifically bound proteins and plasmonic enhancement of fluorescence to reduce background noise

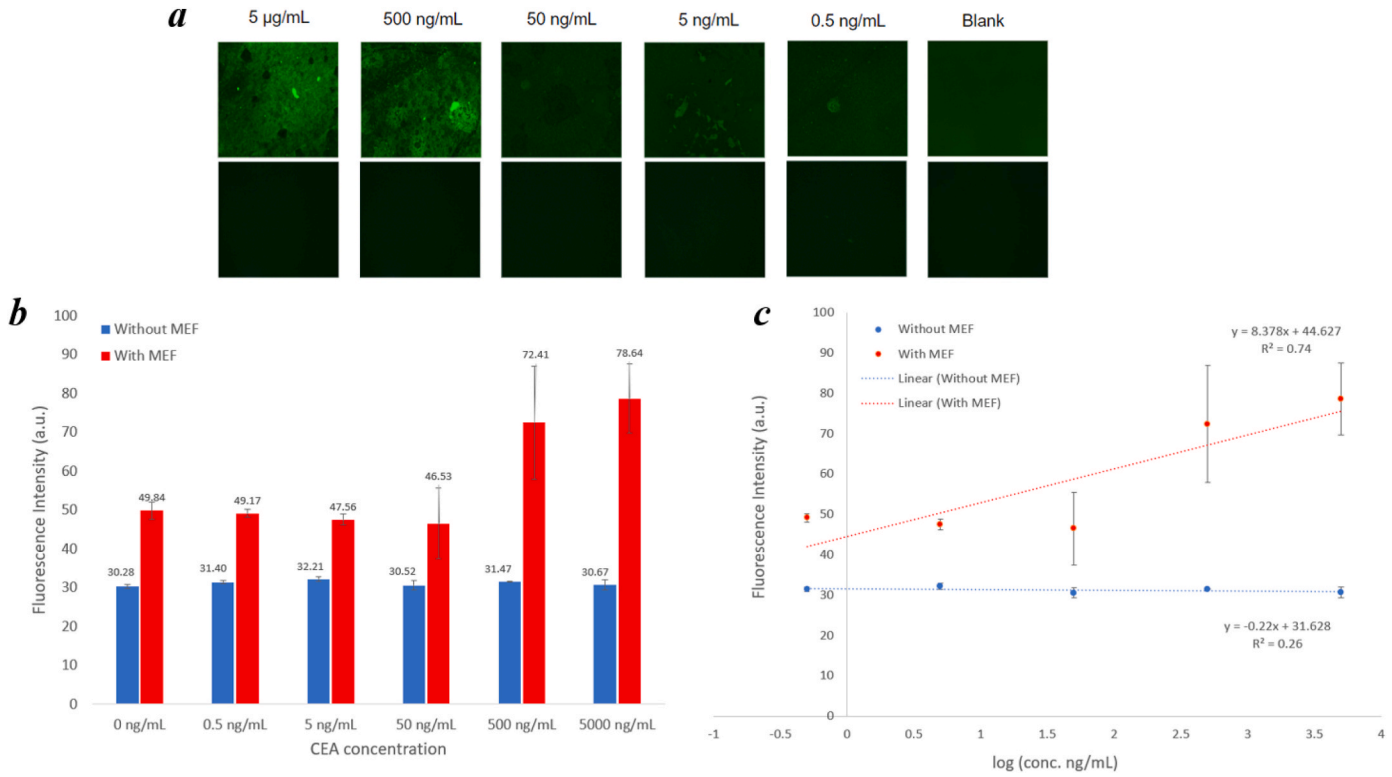

Fig. 5. Results of MEF experiments for CEA diluted in human plasma: a) fluorescence images. Top row of images are fluorescence images with plasmonic region, and bottom row of images are controls. The concentrations of CEA used were 5 μg/mL, 500 ng/mL, 50 ng/mL, 5 ng/mL, 500 pg/mL, and blank plasma sample; b) fluorescence intensities; c) calibration curve for logarithmic concentration from 0.01 to 10000 ng/mL.

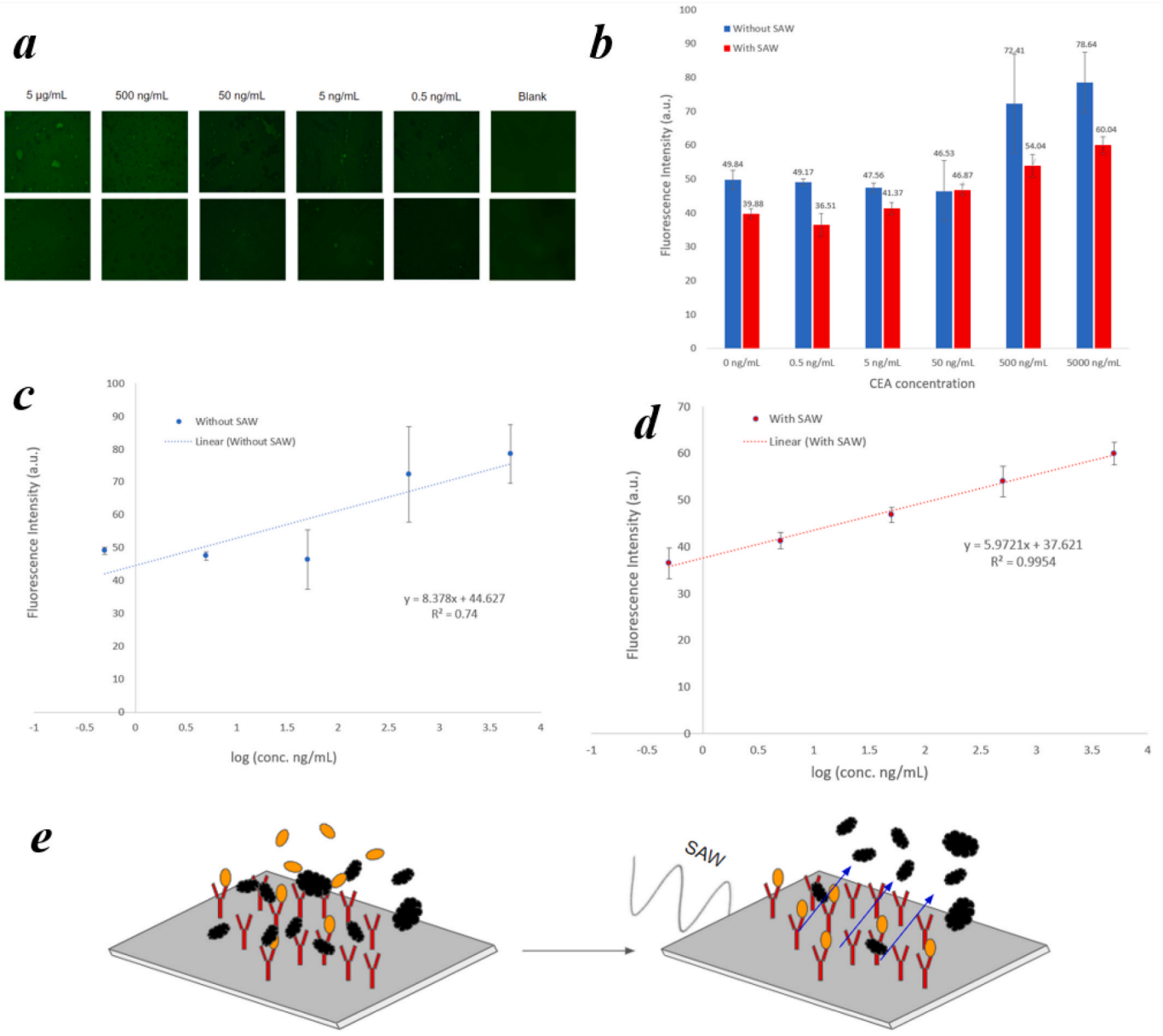

Fig. 6. CEA quantification in human plasma w/o SAW nonspecific binding removal: a) fluorescence images. Top row of images are fluorescence images without SAW removal, and bottom row are fluorescence results with SAW removal. The concentrations of CEA used were 5 μg/mL, 500 ng/mL, 50 ng/mL, 5 ng/mL, 500 pg/mL, and blank plasma sample; b) fluorescence intensities; c) calibration curve for CEA quantification without nonspecific binding removal with SAW from 0.5 to 5000 ng/mL; d) calibration curve with SAW removal; e) Schematic diagram of NSB removal process with SAWs. Target CEA antigens (dark yellow) in human plasma containing non-specific proteins (black). NSB happens when a non-specific protein attaches to the capture antibody (red) or the sensor surface. The right diagram shows SAW streaming to lift NSB proteins and mix them into the PBS stream.

from a complex protein solution and to enhance the fluorescence signal from CEA antigens, sensitivities of immunofluorescence assays are improved. FDTD simulations with experimental results are presented to validate the optimization of silver nanoparticle based plasmonic structures, and a reliable large-scale nanostructure fabrication method is utilized to achieve such nanostructures. The sensor sensitivity was enhanced by a factor of 49.99 using the silica-coated silver nanoparticles based plasmonic structure, and the limit of detection of CEA antigen in human plasma was brought down to 11.81 ng/mL by removing non-specifically bound proteins at the plasmonic modified bio-assembly region. These results provide great potential towards achieving a low-cost, small-size biomarker detection system that allows clinically relevant biomarker quantification directly from untreated body fluids utilizing a very small sample, enabling point of need sensing at clinically relevant concentrations.

CRediT authorship contribution statement

Yuqi Huang: Conceptualization, Methodology, Software, Formal analysis, Validation, Investigation, Writing – original draft, Writing – review & editing. **Shuangming Li:** Conceptualization, Methodology, Writing – review & editing. **Venkat Bhethanabotla:** Conceptualization, Methodology, Resources, Writing – review & editing, Supervision.

Declaration of competing interest

The authors declare that they have no known competing financial interests or personal relationships that could have appeared to influence the work reported in this paper.

Data availability

Data will be made available on request.

Acknowledgement

This work was funded by the National Science Foundation (Grant No. CMI-2108795), which is gratefully acknowledged. The authors declare the following competing financial interests: VRB has financial interest in SenserTec, which develops the technology described in this manuscript.

Appendix A. Supplementary data

Supplementary data to this article can be found online at https://doi.org/10.1016/j.bios.2022.114822.

References

Ahirwar, R., Bariar, S., Balakrishnan, A., Nahar, P., 2015. BSA blocking in enzyme-linked immunosorbent assays is a non-mandatory step: a perspective study on mechanism of BSA blocking in common ELISA protocols. RSC Adv. 5.

Ansys/Lumerical, 2021. Ansys-Lumerical/FDTD. https://support.lumerical.com/hc/en-us/articles/360042161033-Fluorescence-enhancement.

Bharadwaj, P., Novotny, L., 2007. Spectral dependence of single molecule fluorescence enhancement. Opt Express 15 (21), 14266–14274.

Bohlool, B.B., Schmidt, E.L., 1968. Nonspecific staining: its control in immunofluorescence examination of soil. Science 162 (3857), 1012–1014.

Buchwalow, I., Samoilova, V., Boecker, W., Tiemann, M., 2011. Non-specific binding of antibodies in immunohistochemistry: fallacies and facts. Sci. Rep. 1 (1), 28.

Chao, J., DeBiasio, R., Zhu, Z., Giuliano, K.A., Schmidt, B.F., 1996. Immunofluorescence signal amplification by the enzyme-catalyzed deposition of a fluorescent reporter substrate (CARD). Cytometry 23 (1), 48–53.

Cho, Y., Seo, J., Sim, Y., Chung, J., Park, C.E., Park, C.G., Kim, D., Chang, J.B., 2020. FRACTAL: signal amplification of immunofluorescence via cyclic staining of target molecules. Nanoscale 12 (46), 23506–23513.

Choi, H.W., Lee, K.H., Hur, N.H., Lim, H.B., 2014. Cerium oxide-deposited mesoporous silica nanoparticles for the determination of carcinoembryonic antigen in serum using inductively coupled plasma-mass spectrometry. Anal. Chim. Acta 847, 10–15.

Cular, S., Branch, D.W., Bhethanabotla, V.R., Meyer, G.D., Craighead, H.G., 2008. Removal of nonspecifically bound proteins on microarrays using surface acoustic waves. IEEE Sensor. J. 8 (3), 314–320.

Das, P.K., Snider, A.D., Bhethanabotla, V.R., 2020. Acoustic streaming in second-order fluids. Phys. Fluids 32 (12), 123103.

Diagnostics, C., 2022. CEA Serum Rapid Test (Strip). https://www.creative-diagnostics.com/CEA-Serum-Rapid-Test-106462-454.htm.

Duffy, M.J., 2001. Carcinoembryonic antigen as a marker for colorectal cancer: is it clinically useful? Clin. Chem. 47 (4), 624–630.

Galli, C., Coen, M.C., Hauert, R., Katanaev, V.L., Gröning, P., Schlapbach, L., 2002. Creation of nanostructures to study the topographical dependency of protein adsorption. Colloids Surf. B Biointerfaces 26 (3), 255–267.

Grimaldi, I.A., Testa, G., Persichetti, G., Loffredo, F., Villani, F., Bernini, R., 2016. Plasma functionalization procedure for antibody immobilization for SU-8 based sensor. Biosens. Bioelectron. 86, 827–833.

Huang, Y., Das, P.K., Bhethanabotla, V.R., 2021. Surface acoustic waves in biosensing applications. Sensors and Actuators Reports 3, 100041.

Jeong, Y., Kook, Y.-M., Lee, K., Koh, W.-G., 2018. Metal enhanced fluorescence (MEF) for biosensors: general approaches and a review of recent developments. Biosens. Bioelectron. 111, 102–116.

Jeyachandran, Y.L., Mielczarski, J.A., Mielczarski, E., Rai, B., 2010. Efficiency of blocking of non-specific interaction of different proteins by BSA adsorbed on hydrophobic and hydrophilic surfaces. J. Colloid Interface Sci. 341 (1), 136–142.

Lakowicz, J.R., 2006. Principles of Fluorescence Spectroscopy. Springer.

Lamanna, L., Rizzi, F., Bhethanabotla, V.R., De Vittorio, M., 2020. Conformable surface acoustic wave biosensor for E-coli fabricated on PEN plastic film. Biosens. Bioelectron. 163, 112164.

Lertkhachonsuk, A.-a., Buranawongtrakoon, S., Lekskul, N., Rermluk, N., Wee-Stekly, W.-W., Charakorn, C., 2020. Serum CA19-9, CA-125 and CEA as tumor markers for mucinous ovarian tumors. J. Obstet. Gynaecol. Res. 46 (11), 2287–2291.

Li, S., Bhethanabotla, V.R., 2021. Sensitive biosensing using plasmonic enhancement of fluorescence by rapid thermal annealed silver nanostructures. IEEE Sensor. J. 21 (14), 15917–15925.

Lichtenberg, J.Y., Ling, Y., Kim, S., 2019. Non-specific adsorption reduction methods in biosensing. Sensors (Basel) 19 (11).

Liu, J., Li, S., Bhethanabotla, V.R., 2018. Integrating metal-enhanced fluorescence and surface acoustic waves for sensitive and rapid quantification of cancer biomarkers from real matrices. ACS Sens. 3 (1), 222–229.

Long, G.L., Winefordner, J.D., 1983. Limit of detection. A closer look at the IUPAC definition. Anal. Chem. 55 (7), 712A–724A.

Meng, Q., Shi, S., Liang, C., Liang, D., Xu, W., Ji, S., Zhang, B., Ni, Q., Xu, J., Yu, X., 2017. Diagnostic and prognostic value of carcinoembryonic antigen in pancreatic cancer: a systematic review and meta-analysis. OncoTargets Ther. 10, 4591–4598.

Ness, J.M., Akhtar, R.S., Latham, C.B., Roth, K.A., 2003. Combined tyramide signal amplification and quantum dots for sensitive and photostable immunofluorescence detection. J. Histochem. Cytochem. 51 (8), 981–987.

Odell, I.D., Cook, D., 2013. Immunofluorescence techniques. J. Invest. Dermatol. 133 (1), e4.

Sankaranarayanan, S.K., Cular, S., Bhethanabotla, V.R., Joseph, B., 2008. Flow induced by acoustic streaming on surface-acoustic-wave devices and its application in biofouling removal: a computational study and comparisons to experiment. Phys. Rev. E - Stat. Nonlinear Soft Matter Phys. 77 (6 Pt 2), 066308.

Sankaranarayanan, S.K.R.S., Singh, R., Bhethanabotla, V.R., 2010. Acoustic streaming induced elimination of nonspecifically bound proteins from a surface acoustic wave biosensor: mechanism prediction using fluid-structure interaction models. J. Appl. Phys. 108 (10), 104507.

Vaidyanathan, R., van Leeuwen, L.M., Rauf, S., Shiddiky, M.J.A., Trau, M., 2015. A multiplexed device based on tunable nanoshearing for specific detection of multiple protein biomarkers in serum. Sci. Rep. 5 (1), 9756.